Study on dynamic strength and liquefaction mechanism of silt soil in Castor earthquake prone areas under different consolidation ratios

Jiang Chunlin[1], Wang Guangjin[1,2]*, Li Shujian[3], Kang Fuqi[1], Cai Binting[3] and Zhao Lei[3]

[1]Faculty of Land Resources Engineering, Kunming University of Science and Technology, Kunming, China, [2]Yunnan International Technology Transfer Center for Mineral Resources Development and Solid Waste Resource Utilization, Kunming, China, [3]Yunnan Phosphate Group Co., Ltd., Kunming, China

Under the Castor earthquake, there is a risk of liquefaction instability of saturated tailings, and the evolution of dynamic pore pressure can indirectly reflect its instability process. Before applying dynamic loads, the static stress state of soil is one of the main factors affecting the development of soil dynamic strength and dynamic pore pressure, and there are significant differences in soil dynamic strength under different consolidation ratios. This paper conducted dynamic triaxial tests on saturated tailings silt with different consolidation ratios, and analyzed the dynamic strength variation and liquefaction mechanism of the samples using the discrete element method (PFC3D). The results showed that 1) as the K_c' gradually increased, and there was a critical consolidation ratio K_c' during the development of the dynamic strength of the sample. The specific value of K_c' was related to the properties and stress state of saturated sand. The K_c' in this research was about 1.9. When $K_c < 1.9$, dynamic strength was increased with the increase in K_c; when $K_c > 1.9$, dynamic strength was decreased with the K_c. 2) Under the impact of cyclic load, when samples were normally consolidated ($K_c = 1$), the pore water pressure would tend to be equal to the confining pressure to cause soil liquefaction. In the case of eccentric consolidation ($K_c > 1$), the pore water pressure would be less than the confining pressure, thus, the soil liquefaction would not be induced, and the pore pressure value would decrease with the increase of consolidation ratio. This paper provides engineering guidance value for the study of dynamic strength and liquefaction mechanism of tailings sand and silt in Castor earthquake prone areas under different consolidation ratios.

KEYWORDS

Castor earthquake area, saturated tailings sand soil, consolidation ratio, dynamic triaxial test, particle flow simulation

1 Introduction

As is well known, The pre-earthquake action of the on-site soil unit has vertical effective force force σ_v and horizontal effective stress $K_0\sigma_v$ (K_0 is the coefficient of static earth pressure), the earthquake will cause repeated cyclic action of the dynamic shear stress $\pm \tau_d$, while the normal stresses remain constant. Any indoor dynamic test instrument should simulate such a stress state where there is a constant normal stress and a reciprocal shear stress acting on a plane of the soil sample. In the dynamic triaxial test, the stress state in the specimen the stress state in the 45° plane is simulated: for horizontal ground, the initial shear stress $\tau_0 = 0$, using isobaric consolidation K_c, i.e., equal consolidation pressure is applied on the specimen force $\sigma_{1c} = \sigma_{3c} = \sigma_0$, the normal stress in the 45° plane is σ_0, the tangential stress $\tau_0 = 0$. The pre-earthquake stress state can be simulated; for inclined ground, the initial shear stress $\tau_0 \neq 0$, and the bias consolidation $K_c \neq 1$ (K_c is the consolidation stress ratio). The static stress state of the soil before the dynamic load is applied determines the consolidation condition of the indoor.

As shown in Figure 1, The Karst landform area in southwestern China is prone to earthquakes. The dynamic instability of the tailings dam during the earthquake has gradually been paid attention to (Yan-Qiang et al., 2016); besides, most of the tailings dams are in the state of anisotropic consolidation, so it is important to study the dynamic characteristics of sand with different consolidation ratios (wang and Zhou, 2001).

At present, scholars have studied dynamic strength and the evolution law of dynamic pore water pressure of soil different consolidation ratios K_c, and some representative results have been obtained. Through the undrained dynamic triaxial test, Konstadinou, M. (Konstadinou and Georgiannou, 2013). found that the cyclic strength of Ottawa sand increased with the increase of consolidation stress ratio, and obvious stress dependence of sand was observed under high consolidation stress ratio. Through conducting dynamic triaxial tests on Yunlin sand samples with different consolidation ratios ($K_c = 1.0, 1.5, 2.0, 2.5, 3.0$), Chien, LK (Chien et al., 2000) found that liquefaction strength will decrease with the increase of consolidation stress ratio, and under low consolidation ratio ($K_c = 1.5$), the liquefaction strength is very close; when the strain amplitude is small, the influence of K_c tends to be less. Bao Chenyang (Chen-Yang et al., 2006) studied Yunnan silt samples under different consolidation ratios, and found that the dynamic strength curves had the highest point, and this point corresponded to $K_c = 2.1$ and $K_c = 2.01$ respectively when $\sigma_3 = 200kPa$ and $\sigma_3 = 100kPa$. By conducting dynamic triaxial tests on Fujian standard sand under different consolidation ratios of $K_c = 1.0, 1.25, 1.5, 2.0, 2.5, 3.0$, Ma Meiying (Mei-Ying, 1988) concluded that the dynamic strength of sand increases with the increase of K_c in a certain range of K, but the increase of dynamic strength gradually decrease, and the dynamic strength decreases When $K_c = 3.0$. By analyzing the dynamic triaxial test results of unsaturated fly ash, Zhang Jianhong et al. (Zhang and Chang-Rong, 1994) found when $K_c = 1.5$, the dynamic strength was increased compared to that when $K_c = 1.0$, the dynamic strength has shown a downward
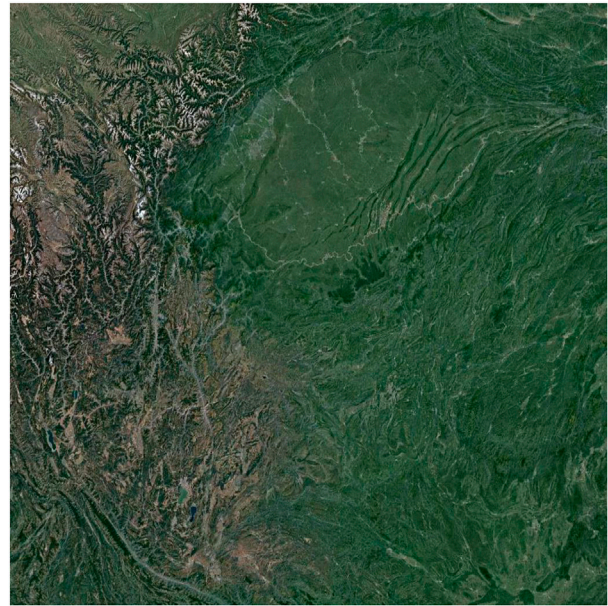

FIGURE 1
Karst landform area.

trend when $K_c = 2.0$. He Changrong et al. () used the Pubugou dam foundation sand to carry out dynamic triaxial tests under consolidation stress ratios of $K_c = 0.43 \sim 2.0$, and it was indicated that the dynamic strength had been increasing. Liao Hongjian et al. (Hong-Jian et al., 1998; Liao et al., 2001) conducted dynamic triaxial tests on Pozzolanic clay under consolidation stress ratios of $K_c = 1.0, 1.5, 2.0, 3.0$, and it was concluded that the dynamic strength tended to be stable with the consolidation ratio. Hu Yuanfang (Hu, 1996) conducted dynamic triaxial tests on Beba power plant fly ash under different consolidations of $K_c = 0.4 \sim 3.0$, and the results showed that the dynamic strength reached the maximum value when $K_c = 2.167$. Through the strength test of saturated sand and gravel materials for the earth-rock dam foundation, Zhang Ru (Zhang et al., 2006) believed that when the anisotropic consolidation $K_c = 0.7 \sim 1.3$, the final pore pressure of the test soil can reach the confining pressure; when $K_c \geq 1.5$, the final pore pressure reachs the confining pressure when the dynamic stress σ_d is greater than the principal stress difference $\sigma_1 - \sigma_3$. Yu Lianhong et al. (Lian-Hong and Wang, 1999) conducted an experimental study on the relationship between the dynamic pore water pressure and the consolidation ratio K_c of saturated silty soil, and concluded that the dynamic pore pressure may still rise to the confining pressure when the K_c is greater than 1.0 and less than a certain value. Nie Shouzhi et al. (Shou-Zhi, 1980) conducted liquefaction tests on saturated sandy soils under different consolidation conditions and proposed a series of indexes such as pore water pressure and dynamic strength, and also analyzed and explained the "notch" in the crest of the dynamic pore water pressure process line. Zhang Kexu et al. (Ke-Xu, 1984)proposed round-trip shear action functions under different consolidation and gave a unified interpretation of

FIGURE 2
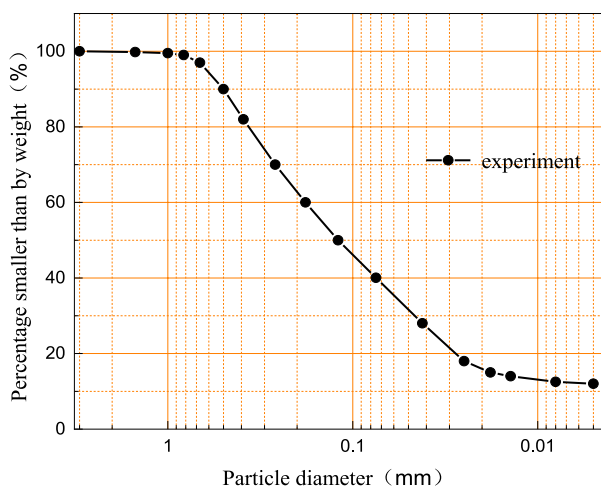KTL-DYN10 dynamic triaxial equipment.

FIGURE 3
Particle size distribution of Tailing silty sand.

the results of several existing liquefaction tests. Wang Yuanzhan et al. (Wang et al., 2015)analyzed the pore pressure development law and undrained shear strength weakening law under the effect of different stress combinations by indoor dynamic triaxial tests with surrounding pressure, initial static deflection stress, cyclic dynamic stress and number of cycles as the test variables, taking Yantai port *in situ* silty powder clay as the research object.

However, during studying ynamic characteristics of soil, the dynamic pore pressure evolution of tailings under different consolidation conditions has not been paid enough attention. In practical projects, the dynamic failure process and dynamic pore pressure evolution law of tailings under different consolidation conditions also have certain differences (ZHANG et al., 2018). Therefore, in this paper, the influence of different consolidation ratios K_c on soil dynamic characteristics was mainly studied. On the basis of existing research, through dynamic triaxial test and discrete element simulation (DAI et al., 2013; KONG et al., 2013; SHEN et al., 2015; JIANG et al., 2020), the macro mechanical behavior and micro mechanical properties of saturated tailing silt were carefully studied according to the macro and micro results; moreover, the test of tailing silt was designed to discuss the influence of K_c on the dynamic strength and dynamic pore pressure of soil samples, and made a reasonable explanation.

2 Experiment scheme

2.1 Experiment apparatus and material

As shown in Figure 2, KTL-DYN10 dynamic triaxial equipment was selected for this experiment, and its hardware system consists of axial loading equipment, a controlling chamber of dynamic confining pressure, a back pressure controller, 8-channel high-speed control and acquisition equipment; The software system is a DSP high-speed digital control system with a maximum operating frequency of 10 Hz and a maximum dynamic stress amplitude of ±10 kN.

In this research, the tailings silty sand was taken from an iron tailings pond in Sichuan, and it is the main damming material of the tailings dam. Figure 3 shows the grading analysis of the tailings

FIGURE 4
Test sample.

samples, the sample used in this test is Void ratio e =0.69, Specific Gravity G=2.725, The dry density of the sample after consolidation is controlled as ρ_d =1.63 g/cm³.

2.2 Sample preparation

In the process of sample preparation, according to the 《Code for Geotechnical Test: GBT 50123-2019》 (General Institute of Water Resources and Hydropower Planning and Design, 2019), the drying temperature was determined to be 110℃. In this test, a cylindrical sample with a diameter of 50 mm and a height of 105 mm was processed, which was compacted in four layers; at the same time, the sample density was controlled according to the dry density, and the dry density of samples was determined to be 1.63 g/cm³ according to the deposition law of the tailings pond. Then, prepared samples were installed as shown in Figure 4.

2.3 Test procedure and scheme

After the sample preparation, the first action was to use the back-pressure controller to test its air impermeability, and then the CO_2 saturation, water head saturation, and back-pressure saturation were subsequently performed to improve the sample saturation. After the sample saturation reached 98% (B>0.98), it was consolidated under the corresponding conditions; After that,

the cyclic load with fixed frequency was applied for the test under the undrained condition.

In this test, the load frequency was set as 1 Hz, the dynamic stress was set as 70 kPa, the consolidation confining pressure was kept to be 100 kPa, and the cyclic load was subjected using the method of equal stress amplitude. For the isotropic consolidation ($K_c = 1$), the consolidation stress was loaded at one time; for the anisotropic consolidation ($K_c > 1$), the consolidation stress was loaded step-wise. The effect of different consolidation ratios on the dynamic characteristics of saturated tailing silty sand was studied by applying different axial static stresses, and the test scheme is shown in Table 1. In order to facilitate analysis and comparison, the failure strain was taken as the criterion for terminating the test in this paper: the failure strain of isotropic consolidation ($K_c = 1$) was defined as 5% of the dynamic strain ($\varepsilon_d = 5\%$), and that of anisotropic consolidation ($K_c > 1$) ws defined as 5% of the total strain (including residual strain and dynamic strain)($\varepsilon = 5\%$) (Mei-Ying, 1980), while the limit equilibrium failure criterion was adopted in the theoretical analysis.
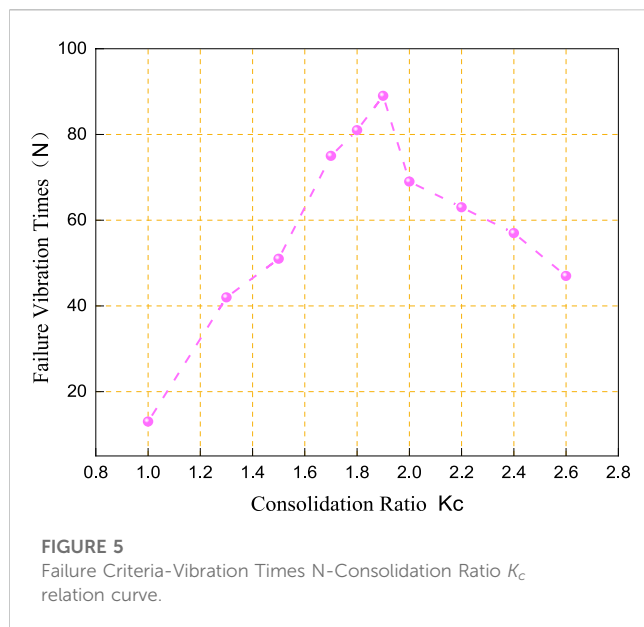
3 Analysis of test results

3.1 The influence of K_c on soil dynamic strength

As shown in Figure 5, When $K_c = 1.0 \sim 1.9$, the higher the K_c, the more vibration times the sample needs to meet the failure standard; When $K_c = 1.9 \sim 2.6$, the changing rule was opposite to the above; Therefore, it can be seen that the influence of the consolidation ratio K_c on the dynamic strength of soil samples is very obvious. When $K_c = 1.0 \sim 2.6$, the value of 1.9 was the turning point; when $K_c < 1.9$, dynamic strength gradually increased; when $K_c > 1.9$, dynamic strength first increased and then decreased. Thus, the existence of critical consolidation ratio is proved. When $K_c = 1$, the initial shear stress was zero, the reverse shear stress was the maximum, and the soil particle skeleton was in a certain equilibrium state. The cyclic load made the direction of the large principal stress axial rotated 90°, and the cyclic shear stress made the pore space uniformly distributed, which resulted in the occurrence of plastic compaction, and the increase in pore pressure due to the sliding of particle skeleton. When $1 < K_c < 1.9$, the initial shear stress increased with K_c, and the shear effect was induced during the test, which made the sand particles be rearranged and the deformation of the soil particle skeleton in a more stable state due to the disturbance of shear on the sand particle skeleton. The reverse shear stress slowly decreased with K_c, its influence on the change of pore space and volume of samples decreased gradually during vibration, as well as the deformation rate and amplitude, thus the seismic stability and liquefaction resistance became higher. As shown in Figure 6, I, II and III represent stress circles under different consolidation ratios, ①, ②, ③ represents the distance between consolidation stress circle and strength envelope; It can be seen that ③<②<①. This indicates that when $K_c > 1.9$, the greater the difference between σ_1 and σ_3, the larger the initial shear stress, the larger the diameter of the molar circle during static consolidation, and the less the distance from the Mohr-Coulomb envelope. For larger K_c, even if a periodic load with small amplitude σ_d was applied, the soil sample would also be

TABLE 1 Test scheme.

Test number	Confining pressure/kPa	Consolidation ratio	Frequency/Hz	Dynamic stress/kPa
1	100	1	1	70
2		1.3		
3		1.5		
4		1.7		
5		1.8		
6		1.9		
7		2.0		
8		2.2		
9		2.4		
10		2.6		

FIGURE 5
Failure Criteria-Vibration Times N-Consolidation Ratio K_c relation curve.

FIGURE 6
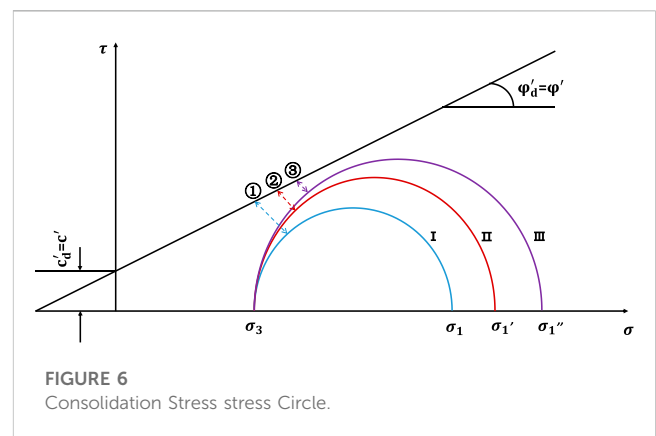Consolidation Stress stress Circle.

deformed or damaged quickly; even without the dynamic load, the specimen would also occur shear failure as the static load was continuously applied by increasing σ_1.

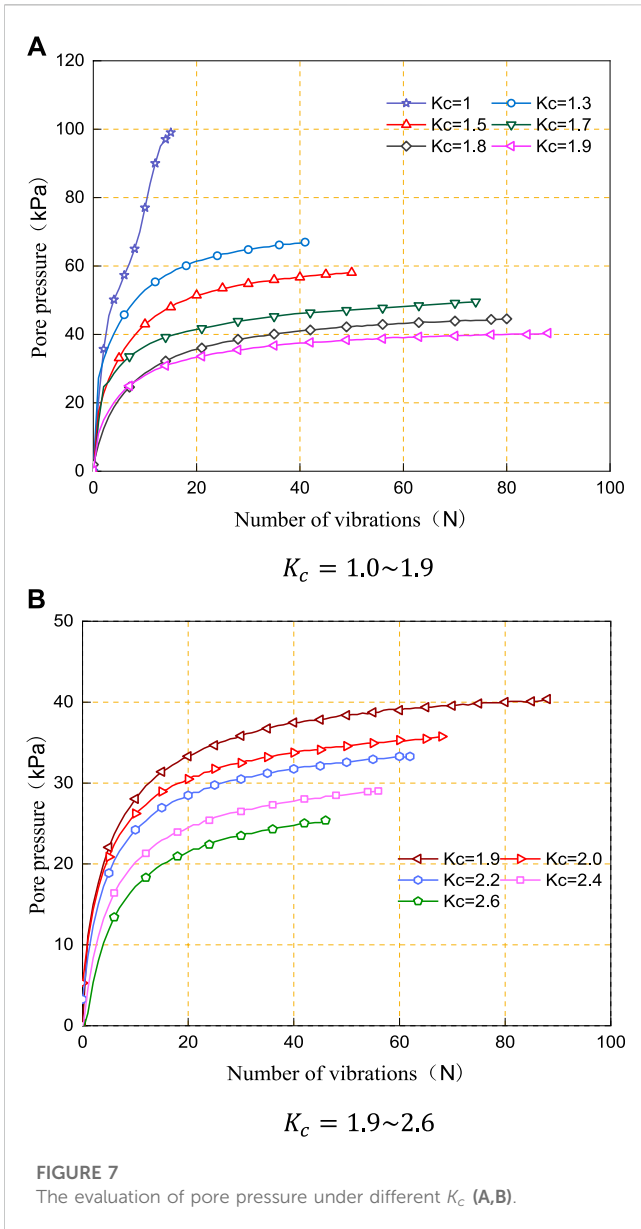## 3.2 The influence of K_c on soil dynamic pore pressure

Figure 7 shows development curves of dynamic pore water pressure of the sample under different consolidation ratios K_c, it can be seen that when $K_c = 1$, the pore pressure would finally reach the confining pressure and realize complete liquefaction; When $K_c > 1$, the pore pressure would always be less than the confining pressure, and the initial liquefaction would not be caused; besides, the larger the consolidation ratio, the smaller the pore pressure.

In order to analyze the influence of different consolidation ratios on the evolution of dynamic pore pressure of tailing silty sand, this paper used the limit equilibrium criterion to analyze the pore water pressure of materials under the limit equilibrium state, namely, the critical pore water pressure u_{cr} (Ding-Yi et al., 1981; Li et al., 2021a; Liu et al., 2022; Zhou et al., 2022). It was assumed that the static limit equilibrium condition was also applicable to the dynamic test, and their Mohr-Coulomb failure envelopes were the same, which means the dynamic effective cohesion c_d' and internal friction angle φ_d' was respectively equal to static effective cohesion c' and internal friction angle φ' as shown in Figure 7. The stress circle ① represents the stress state of the sample before vibration, and the stress circle ② represents the maximum stress circle during dynamic load application, that is, the dynamic stress was equal to the instantaneous stress circle with an amplitude of σ_d. During the process of dynamic loading, the pore water pressure in the sample would develop continuously, and the stress circle ② would move towards the strength envelope; when the pore water pressure reached the critical value u_{cr}, the stress circle was tangent to the strength envelope, suggesting that the tailing silty sand reached the failure state according to the limit equilibrium condition.

According to the geometric conditions shown in Figure 8, the pore water pressure at the limit equilibrium state can be deduced as follows.

FIGURE 7
The evaluation of pore pressure under different K_c **(A,B)**.

$$u_{cr} = \frac{\sigma_1 + \sigma_3}{2} + \frac{c'}{tan\,\varphi'} - \frac{\sigma_1 - \sigma_3 + \sigma_d\left(1 - sin\,\varphi'\right)}{2\,sin\,\varphi'} \qquad (1)$$

Where: c' and φ' is the static effective cohesion and static effective internal friction angle of soil samples; σ_d is the dynamic stress amplitude; σ_1 and σ_3 represents axial pressure and confining pressure respectively.
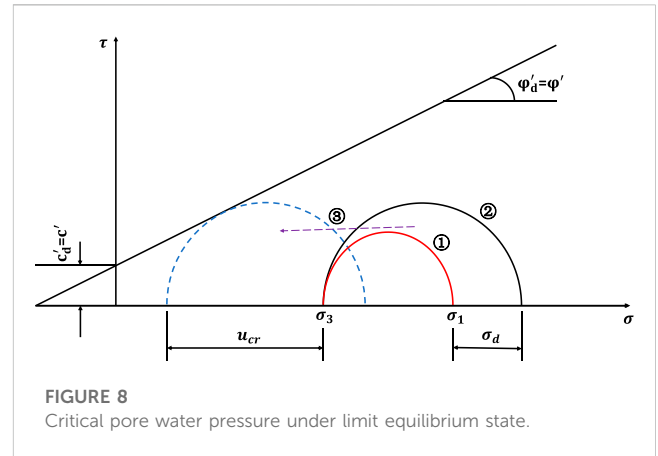
Setting $\sigma_1 = K_c\sigma_3$, it can be obtained:

$$u_{cr} = \left(\frac{K_c + 1}{2} + \frac{K_c - 1}{2\,sin\,\varphi'}\right)\sigma_3 + \frac{c'}{tan\,\varphi'} + \frac{\sigma_d\left(sin\,\varphi' - 1\right)}{2\,sin\,\varphi'} \qquad (2)$$

making

$$\lambda = \frac{K_c + 1}{2} + \frac{K_c - 1}{2\,sin\,\varphi'} \qquad (3)$$

λ is the critical pore pressure ratio

FIGURE 8
Critical pore water pressure under limit equilibrium state.

$$\Delta\sigma = \frac{c'}{tan\,\varphi'} + \frac{\sigma_d\left(sin\,\varphi' - 1\right)}{2\,sin\,\varphi'} \qquad (4)$$

then

$$u_{cr} = \lambda\sigma_3 + \Delta\sigma \qquad (5)$$

For common tailings, when $\sigma_d = 30kPa$, $\Delta\sigma \approx 0$; when $\sigma_d > 30kPa$, $\Delta\sigma < 0$, and it decreased with the increase in σ_d.

When $K_c = 1$, by substituting, $u_{cr} = \sigma_3 + \Delta\sigma$; when $K_c > 1$, aftering substituting $\lambda = 1$, the following can be gotten:

$$\lambda = \frac{K_c + 1}{2} + \frac{K_c - 1}{2\,sin\,\varphi'} = \frac{1 + sin\,\varphi'}{2\,sin\,\varphi'} - \frac{1 - sin\,\varphi'}{2\,sin\,\varphi'}K_c \qquad (6)$$

Because $0 < sin\,\varphi' < 1$, the critical pore pressure ratio λ decreased with the increase of consolidation stress ratio K_c. After substituting Eq. 6, When $K_c > 1$, the critical pore pressure ratio $\lambda < 1$, and

$$u_{cr} < \sigma_3 + \Delta\sigma \qquad (7)$$

Therefore, for a given dynamic stress amplitude, the pore water pressure will approach the confining pressure during isobaric consolidation, and during anisotropic consolidation, the critical pore pressure will be e less than the confining pressure, and the larger the consolidation ratio, the smaller the critical pore pressure.

4 Microscopic analysis

4.1 The introduction of simulation

In this paper, PFC 3D was used to simulate the standard indoor undrained dynamic triaxial test of saturated tailing silty sand, and the simulated effective confining pressure was controlled to be 100 kPa; the test was carried out using the loading method of equal stress amplitude. The upper and lower walls are loaded uniformly by the control program, and when the bias stress reaches the set stress amplitude q_{cyc}, the upper and lower walls reverse and continue to move until they reach the set stress amplitude q_{cyc} in the opposite direction and then reverse again.
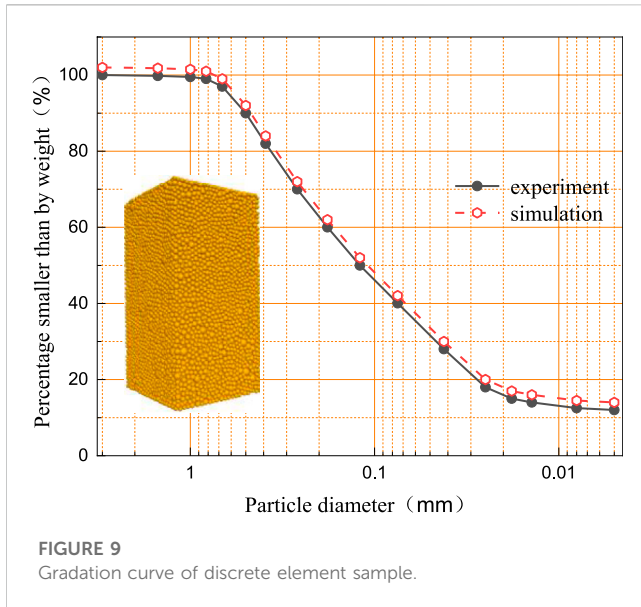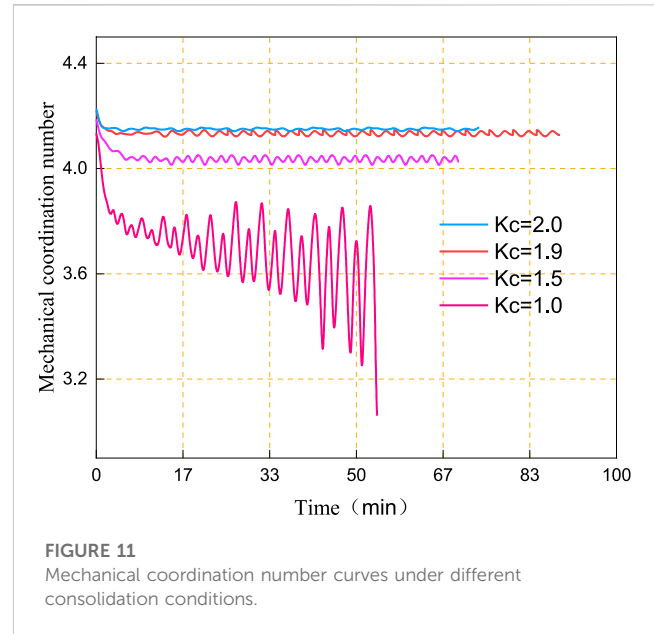
FIGURE 9
Gradation curve of discrete element sample.

FIGURE 11
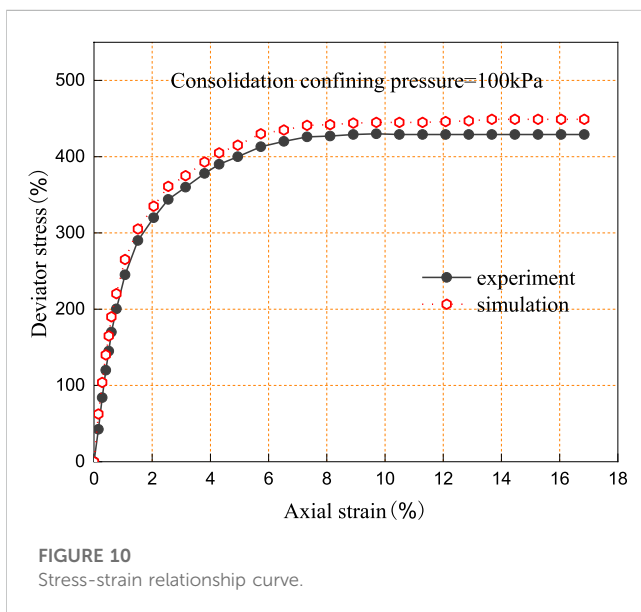Mechanical coordination number curves under different consolidation conditions.

FIGURE 10
Stress-strain relationship curve.

TABLE 2 Parameters of the discrete element model.

Microscopic parameter	Value
Stiffness modulus	1×10^8
Stiffness ratio	1.0
Friction coefficient	0.5
density	2650
Anti-rotation coefficient	0.5

During the loading process, the lateral strain ε_1 is equal to the axial strain $-\varepsilon_2$ by adjusting the movement rate of the lateral walls, at which time the specimen volume is kept constant, and

this constant volume condition is comparable to the undrained condition in the conventional cyclic triaxial test.Based on the constant volume condition, the liquefaction characteristics of the sample were simulated (ZHOU et al., 2009). The advantage of particle flow numerical simulation is the ability to observe the evolution of the meso fabric parameters in the sample at different cyclic loading times while modelling macroscopic mechanical performance of sample liquefaction; thus, the internal relationship between the change of meso fabric and the macroscopic mechanical response in the process of sand liquefaction can be analyzed, so as to further explore the meso-mechanical mechanism of sand liquefaction (Yang et al., 2007; Liu et al., 2020). In this simuation, situations under $K_c = 1.0, K_c = 1.5, K_c = 1.9, K_c = 2.0$ were taken as examples to analyze the coordination number and energy under different consolidation conditions. In this paper, the particle grading of the discrete element sample was determined first, as shown in Figure 9. After that, the stress-strain curve simulated by PFC triaxial shear test was comapred to the results of indoor triaxial shear test to calibrate the reasonable contact model parameters (AHMAD et al., 2019a; Yao-Hui et al., 2021), and these calibtared parameters were adopted for the subsequent dynamic triaxial test simulation and microscopic property analysis (JIANG, 2019). The comparison between numerical simulation and the indoor triaxial shear test is shown in Figure 10, and calibrated physical parameters of numerical model are shown in Table 2.

4.2 Analysis of mechanical coordination number

The mechanical coordination number refers to the average number of contacts per particle in the sample (MAHMOOD et al., 2020; AHMAD et al., 2021), excluding suspended particles with contact numbers less than or equal to 1. For granular
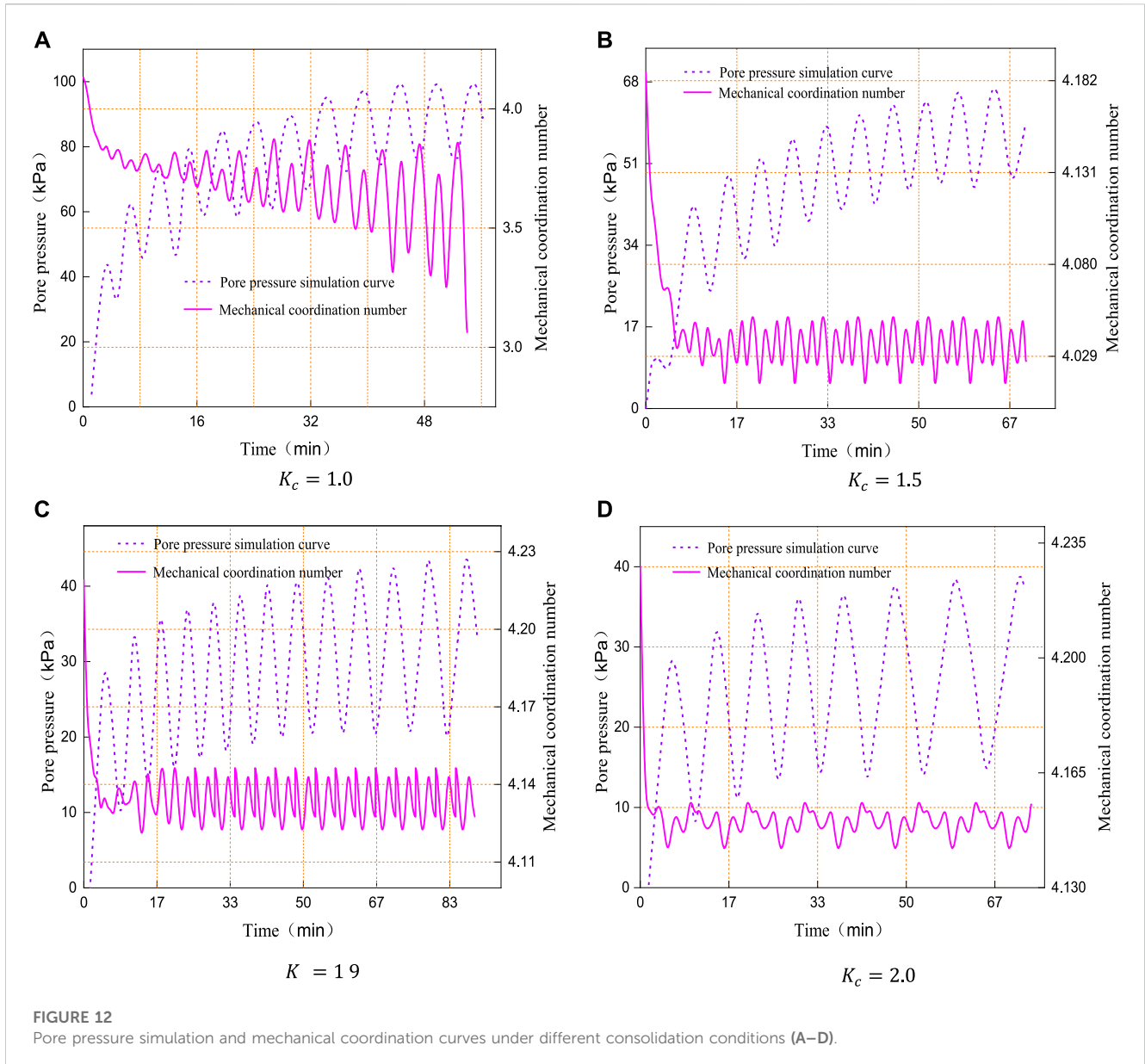
FIGURE 12
Pore pressure simulation and mechanical coordination curves under different consolidation conditions **(A–D)**.

materials, their mechanical properties are mainly affected by the density, which is affected by the indirect contact density of particles at the microscopic level (Thornton, 2000; Li et al., 2021b), which can be expressed by the mechanical coordination number of particles.

It can be seen from Figure 11 that with the increase of the consolidation ratio, the initial value of the mechanical coordination number became larger, as well as the number of particle contacts and the compactness of the sample, at the initial stage of cyclic loading, the mechanical coordination number of the sample continued to decrease. Figure 12 shows the changing curve of the instantaneous dynamic pore water pressure and corresponding mechanical coordination number curve while meeting the failure criteria under different consolidation ratios K_c; it can be seen from Figure 12A, when $K_c = 1$, when the "initial liquefaction" was initiated, and the mechanical coordination

number decreased to about 3, which was reflected by the increase of pore water pressure under the undrained condition at the macroscopic level. At this time, the pore water pressure reached the confining pressure. According to Figures 12B–D, it can be seen that when $K_c = 1.5$, $K_c = 1.9$, $K_c = 2.0$, with the increase of the consolidation ratio, the decreasing amplitude of the mechanical coordination number decreased gradually during the cyclic loading of the sample. When the pore water pressure was stable, the mechanical coordination number did not fluctuate significantly, and the pore water pressure failed to reach the confining pressure. As the consolidation ratio increased from $K_c = 1$, $K_c = 1.5$ to $K_c = 1.9$ the time required for the sample to occur liquefaction became longer r; And from $K_c = 1.9$ to $K_c = 2.0$, with the increase in consolidation ratio, the time required for the sample to reach the failure standard became shorter.

FIGURE 13
Energy curves under different consolidation conditions **(A–D)**.
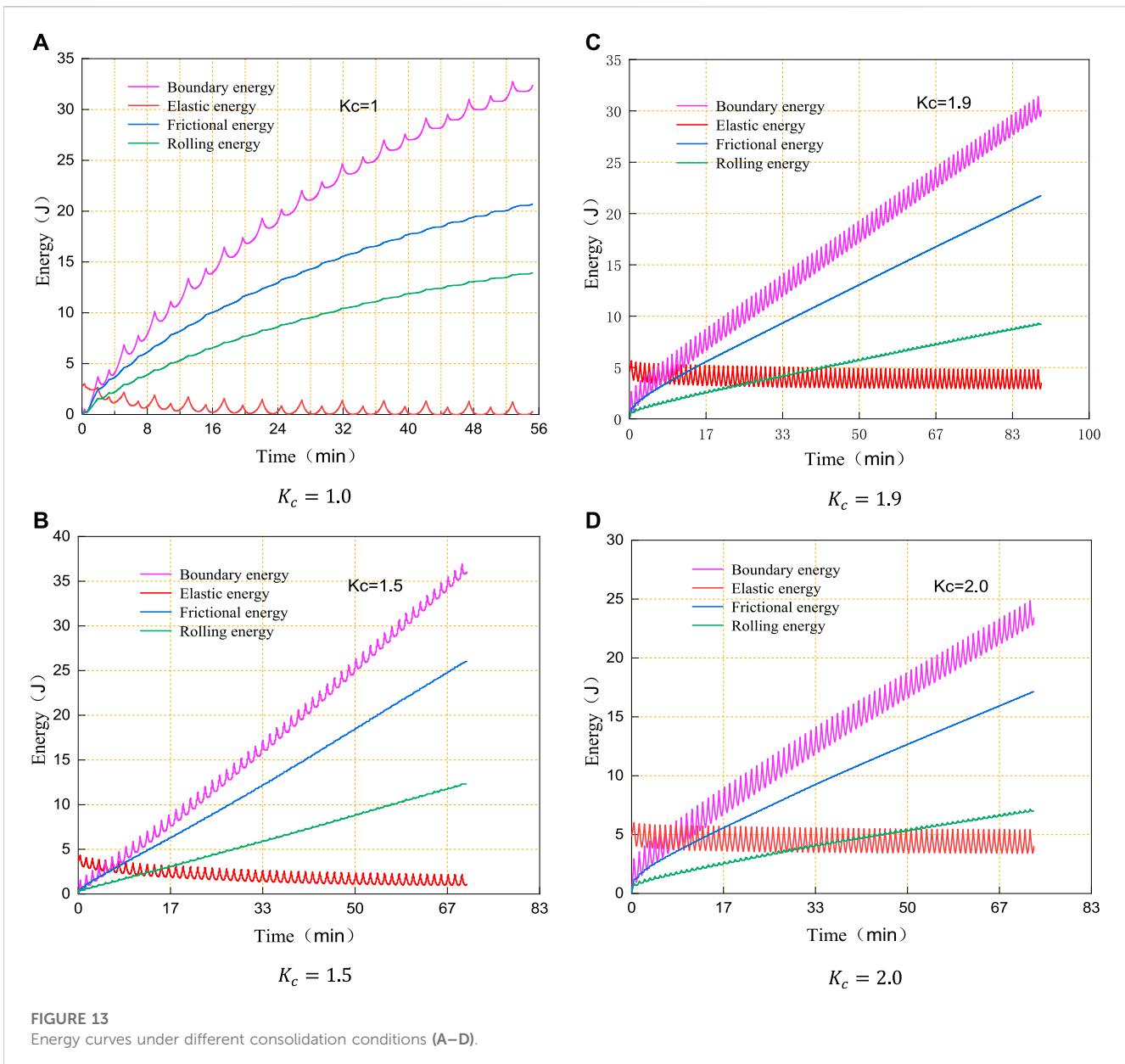
4.3 Energy analysis

The energy storage and dissipation of particles during the loading process can represent their macroscopic mechanical response to a certain extent, and their failure actually experienced the evolution process of energy dissipation and instability (AHMAD et al., 2019b; AHMAD et al., 2020). The following will focus on the evolution law of The evolution law of elastic energy of particles (refers to the energy stored in the contact area of particles to deform the particles), particle friction (Bolton et al., 2008; Li et al., 2023), rolling energy dissipation (refers to the energy dissipated by sliding friction and anti-rolling between particles respectively) and boundary energy (refers to the energy generated by wall driving) (AHMAD et al., 2019c; Gao et al., 2023).

Figure 13 shows the energy evolution curves of the saturated tailing silty sand samples. it can be seen when the wall was subjected to cyclic loading and unloading, the wall would generate a certain amount of energy named boundary energy. At the same time, there was a certain amount of elastic energy stored at the contact of particles, and it increased and decreased successively with the loading and unloading process, but the decreasing amplitude was greater than the increasing amplitude so that the elastic energy was gradually released. In addition, under the effect of cyclic load, relative sliding (friction energy consumption) occurred between particles, which was followed by different degrees of rolling between particles (rolling energy consumption).

At the initial state, the elastic energy of particles increased with the increase of the consolidation ratio. As shown in Figure 13A, when $K_c = 1$, as the cyclic loading was subjected, the elastic energy of particles became 0, and the slope of particle friction dissipation energy and particle bending dissipation energy gradually decreased to approach 0; At this time, the sample began to occur initial

liquefaction. As shown in Figures 13B–D, when $K_c = 1.5, K_c = 1.9, K_c = 2.0$, the particle elastic energy did not decrease to 0, while the particle friction dissipation energy and particle bending dissipation energy continued to increase, without showing signs of initial liquefaction. Moreover, with the increase of the consolidation ratio, the elastic energy of the remaining particles became larger, which was the liquefaction of the sample when $K_c = 1$ on the macro level and pore water pressure reached confining pressure, and when $K_c > 1$, the sample did not occur liquefaction, and the pore water pressure decreased with the increase of consolidation ratio.

5 Conclusion

In this paper, in order to study the dynamic strength and liquefaction mechanism of tailings sand in karst seismic prone areas under different static stress states, a series of dynamic triaxial tests were conducted on saturated tailings fines in an iron tailings pond in Sichuan, and combined with discrete element simulations to further explore the dynamic properties of the fines under different consolidation ratios. The main conclusions are as follows.

(1) The critical consolidation ratio K_c' was proved by dynamic triaxial test and particle flow simulation, and its specific value is related to the properties and stress state of saturated sand. In this research, the critical consolidation stress ratio K_c' was about 1.9.
(2) The variation of dynamic strength showed different trends before and after reaching the $K_c' = 1.9$. When $K_c < 1.9$, the dynamic strength of the sample increased with the K_c; when $K_c > 1.9$, the dynamic strength of the sample decreased with the K_c. (3) The limit equilibrium theory and particle flow simulation were used to explain the phenomenon that for the isobaric consolidation $K_c = 1$, the pore water pressure tended to the confining pressure and induced complete liquefaction. For anisotropic consolidation ($K_c > 1$), the pore water pressure was less than the confining pressure and failed to initiate liquefaction, and decreased with the increase of consolidation ratio.
(3) The limit equilibrium theory and particle flow simulation were used to explain the phenomenon that for the isobaric

consolidation $K_c = 1$, the pore water pressure tended to the confining pressure and induced complete liquefaction. For anisotropic consolidation ($K_c > 1$), the pore water pressure was less than the confining pressure and failed to initiate liquefaction, and decreased with the increase of consolidation ratio.

Data availability statement

The original contributions presented in the study are included in the article/Supplementary material, further inquiries can be directed to the corresponding author/s.

Author contributions

JC: Writing—review and editing WG: Conceptualization LS: Methodology KF: Software CB: Validation ZL: Formal analysis. All authors contributed to the article and approved the submitted version.

Conflict of interest

The authors LS, CB, and ZL were employed by Yunnan Phosphate Group Co., Ltd.

The remaining authors declare that the research was conducted in the absence of any commercial or financial relationships that could be construed as a potential conflict of interest.

Publisher's note

All claims expressed in this article are solely those of the authors and do not necessarily represent those of their affiliated organizations, or those of the publisher, the editors and the reviewers. Any product that may be evaluated in this article, or claim that may be made by its manufacturer, is not guaranteed or endorsed by the publisher.

References

Ahmad, M., Tang, X. W., Qiu, J. N., Gu, W-J., and Ahmad, F. (2020). A step forward towards a comprehensive framework for assessing liquefaction land damage vulnerability: Exploration from historical data. *Front. Struct. Civ. Eng.* 14 (6), 1476–1491. doi:10.1007/s11709-020-0670-z

Ahmad, M., Tang, X. W., Qiu, J. N., Gu, W-J., and Ahmad, F. (2021). Application of machine learning algorithms for the evaluation of seismic soil liquefaction potential. *Front. Struct. Civ. Eng.* 15 (2), 490–505. doi:10.1007/s11709-020-0669-5

Ahmad, M., Tang, X-W., Qiu, J-N., and Ahmad, F. (2019a). Evaluating seismic soil liquefaction potential using bayesian belief network and C4.5 decision tree approaches. *Appl. Sci.* 9 (20), 4226. doi:10.3390/app9204226

Ahmad, M., Tang, X-W., Qiu, J-N., and Ahmad, F. (2019b). Interpretive structural modeling and MICMAC analysis for identifying and benchmarking significant factors of seismic soil liquefaction. *Appl. Sci.* 9 (2), 233. doi:10.3390/app9020233

Ahmad, M., Xiaowei, T., and Jiangnan, Q. (2019c). Response and tolerability of sofosbuvir plus daclatasvir in elderly patients with chronic hepatitis-C. *IEEE 14th Int. Conf. Intelligent Syst. Knowl. Eng. (ISKE) Proc.* 31, 527–529.

Bolton, M. D., Nakata, Y., and Cheng, Y. P. (2008). Micro- and macro-mechanical behaviour of DEM crushable materials. *Geotechnique* 58 (6), 471–480. doi:10.1680/geot.2008.58.6.471

Chang-Rong, H. E. (1998). Compression and extrusion elongation characteristics of the dynamic triaxial test[J]. *Sichuan United Univ. Sci. Ed.* 2(04), 49–54. doi:10.15961/j.jsuese.1998.04.009

Chen-Yang, B. A. O., Xiang-Juan, Y., and Gao, Z. B. (2006). Experimental study on the dynamic properties of Yunnan chalk soil[J]. *J. Disaster Prev. Mitig. Eng.* 26 (03), 321–325. doi:10.13409/j.cnki.jdpme.2006.03.015

Chien, L. K., Oh, Y. N., and Chang, C. H. (2000). "In the effects of anisotropy consolidation on liquefaction strength and deformation for reclaimed soil," in *10th international offshore and polar engineering conference (ISOPE-2000)*. Seattle,Wa; International Society Offshore& Polar Engineers. 594–599. Seattle, Wa May 28-Jun 02.

Dai, B. B., Yang, J., and Zhou, C. Y. (2013). Numerical simulation of unstable behavior of loose sand[J]. *Chin. J. Geotechnical Eng.* 35 (09), 1737–1745.

Ding-Yi, X. I. E., Zhi-Hui, W. U., and Yao-Tang, G. U. O. (1981). Application of limit equilibrium theory in the analysis of dynamic instability process of saturated sand[J]. *China Civ. Eng. J.* 14 (04), 17–28. doi:10.15951/j.tmgcxb.1981.04.003

Gao, Y., Yu, Z., Chen, W., Yin, Q., Wu, J., and Wang, W. (2023). Recognition of rock materials after high-temperature deterioration based on SEM images via deep learning. *J. Mater. Res. Technol.* 25, 273–284. doi:10.1016/j.jmrt.2023.05.271

General Institute of Water Resources and Hydropower Planning and Design (2019). "Ministry of water Resources, nanjing Institute of water Resources science," in *Geotechnical test procedures: Gbt 50123 -2019[S]* (China Plan Press.

Hong-Jian, L., Mao-Hong, Y., and Qi-Ming, W. A. I. (1998). Study of dynamic shear strength of loess-like soils and volcanic ash clayey soils[J]. *J. Xi'an Jiaot. Univ.* 32 (10), 73–77.

Hu, Y. F. (1996). *Engineering properties and stability analysis of fly ash dam construction*. Sichuan United University.

Jiang, M. J., Sun, R. H., and Tao, L. I. (2020). CFD-DEM simulation of undrained cyclic triaxial shear of microbial treated sand[J]. *Chin. J. Geotechnical Eng.* 42 (01), 20–28. doi:10.11779/CJGE202001002

Jiang, Y. X. (2019). *Study on the vibration liquefaction characteristics of gravelly sandy soil and rubbery sandy soil[D]*. China University of Mining and Technology.

Ke-Xu, Z. (1984). Liquefaction stress condition of saturated sand[J]. *Earthq. Eng. Eng. Vib.* 4 (1), 99–109. doi:10.13197/j.eeev.1984.01.009

Kong, L., Liang-Liang, J. I., and Cao, J. F. (2013). Meso-mechanism of the effect of stress path and particle size on sand deformation[J]. *Chin. J. Rock Mech. Eng.* 32 (11), 2334–2341.

Konstadinou, M., and Georgiannou, V. N. (2013). Cyclic behaviour of loose anisotropically consolidated Ottawa sand under undrained torsional loading. *Geotechnique* 63 (13), 1144–1158. doi:10.1680/geot.12.p.145

Li, X. L., Chen, S. J., Liu, S. M., and Li, Z. H. (2021a). AE waveform characteristics of rock mass under uniaxial loading based on Hilbert-Huang transform. *J. Central South Univ.* 28 (6), 1843–1856. doi:10.1007/s11771-021-4734-6

Li, X. L., Chen, S. J., Wang, S., Zhao, M., and Liu, H. (2021b). Study on *in situ* stress distribution law of the deep mine taking Linyi Mining area as an example. *Adv. Mater. Sci. Eng.* 9 (4), 5594181–5594211. doi:10.1155/2021/5594181

Li, X. L., Zhang, X. Y., and Shen, W. L. (2023). Abutment pressure distribution law and support analysis of super large mining height face. *Int. J. Environ. Res. Public Health* 20 (2), 227. doi:10.3390/ijerph20010227

Lian-Hong, Y. U., and Wang, Bo (1999). Experimental study of vibratory pore water pressure in saturated powder soils[J]. *J. Dalian Univ. | J Dalian Univ* 20 (4), 59–64.

Liao, H. J., Song, L., and Zheng, Y. A. N. G. (2001). Experimental study on the strength of cohesive soils under reciprocal loading and the criteria for taking values[J]. *Rock Soil Mech.* 2001 (01), 1620. doi:10.16285/j.rsm.2001.01.004

Liu, H. Y., Zhang, B. Y., Li, X. L., Liu, C., Cheng, W., Feng, W., et al. (2022). Research on roof damage mechanism and control technology of gob-side entry retaining under close distance gob. *Eng. Fail. Anal.* 138 (5), 106331. doi:10.1016/j.engfailanal.2022.106331

Liu, S. M., Li, X. L., Wang, D. K., and Zhang, D. (2020). Investigations on the mechanism of the microstructural evolution of different coal ranks under liquid nitrogen cold soaking. *Energy Sources, Part A Recovery, Util. Environ. Eff.*, 1–17. doi:10.1080/15567036.2020.1841856

Mahmood, A., Tang, X-W., Qiu, J-N., Gu, W-J., and Ahmad, F. (2020). A hybrid approach for evaluating CPT-based seismic soil liquefaction potential using Bayesian belief networks. *J. Central South Univ.* 27 (2), 500–516. doi:10.1007/s11771-020-4312-3

Mei-Ying, M. A. (1988). Effect of initial consolidation shear stress on the dynamic strength of saturated sandy soils[J]. *Water Resour. Water Transp. Sci. Res.* 2 (1), 63–68. doi:10.16198/j.cnki.1009-640x.1988.01.007

Mei-Ying, M. A. (1980). Several problems of standard sand liquefaction test[J]. *Chin. J. Geotechnical Eng.* 2 (4), 46–54.

Shen, Y., Tao, M. A., and Guo-Jian, X. U. (2015). PFC numerical experimental study on dynamic collapse characteristics of silt under stress control mode[J]. *Chin. J. Geotechnical Eng.* 37 (12), 2280–2285.

Shou-Zhi, N. E. I. (1980). Liquefaction and strength of saturated sand under dynamic load[J]. *Chin. J. Geotechnical Eng.* (03), 64–73.

Thornton, C. (2000). Numerical simulations of deviatoric shear deformation of granular media. *Geotechnique* 50 (1), 43–53. doi:10.1680/geot.2000.50.1.43

Wang, X. H., and Zhou, H. L. (2001). Influence of consolidation ratio on liquefaction of saturated sand[J]. *China Railw. Sci.* 22 (6), 121–126.

Wang, Y. Z., Pan-Bo, Y. A. N. G., and Sun, Xi-Ping (2015). Study on strength weakening of soft clay under cyclic load and its dynamic calculation application[J]. *Chin. J. Geotechnical Eng.* 37 (05), 821–828. doi:10.11779/CJGE201505007

Yan-Qiang, D. U., Chun-He, Y. A. N. G., and Shang-Wei, W. U. (2016). Pore water pressure characteristics of tailings silt undercyclic loading[J]. *J. Northeast. Univ. Sci.* 37 (04), 583–588. doi:10.3969/j.issn.1005-3026.2016.04.027

Yang, L. I. U., Zhou, J., and Wu, S. C. (2007). Fine view numerical simulation of sandy soil deformation under cyclic loading I:Loose sand test results[J]. *Chin. J. Geotechnical Eng.* 29 (7), 1035–1041.

Yao-Hui, G. U. O., Peng, Z., and Tian, Y. K. (2021). Numerical simulation of particle flow in triaxial compression of tailings from a metal mine[J]. *Min. Res. Dev.* 41 (05), 118–123. doi:10.13827/j.cnki.kyyk.2021.05.021

Zhang, J. H., and Chang-Rong, H. E. (1994). Liquefaction strength and pore pressure law of unsaturated sandy soils under reciprocal loading[J]. *J. Chengdu Univ. Sci. Technol.* (01), 1–8.

Zhang, Ru, Chang-Rong, H. E., Wen-Ping, F. E. I., and Mingzhong, G. A. O. (2006). Effect of consolidation stress ratio on the development pattern of dynamic strength and dynamic pore pressure of soil samples[J]. *Chin. J. Geotechnical Eng.* (01), 101–105.

Zhang, X. Z., Shang-Wei, W. U., and Zhang, Chao (2018). Evolution of dynamic pore pressure in tailings under different consolidation conditions[J]. *Rock Soil Mech.* 39 (03), 815–822. doi:10.16285/j.rsm.2016.0921

Zhou, J., Yang, Y. X., and yang, L. I. U. (2009). Numerical simulation of granular flow with sandy soil liquefaction characteristics under cyclic loading[J]. *Rock Soil Mech.* 30 (04), 1083–1088. doi:10.16285/j.rsm.2009.04.053

Zhou, X. M., Wang, S., Li, X. L., Meng, J., Zhang, L., Pu, D., et al. (2022). Research on theory and technology of floor heave control in semicoal rock roadway: Taking longhu coal mine in Qitaihe mining area as an Example. *Lithosphere* 2022 (11), 3810988. doi:10.2113/2022/3810988